Grant agreement No. 764810

Science for Clean Energy

H2020-LCE-2017-RES-CCS-RIA
Competitive low-carbon energy

D6.2
Proof of concept laboratory demonstration of EIT based sensing skin for well cap structures

WP 6 – Implementation of Novel Technologies

Due date of deliverable	31/08/2019 (Month 24)
Actual submission date	16/10/2019 (Month 26)
Start date of project	01/09/2017
Duration	36 months
Lead beneficiary	UEF
Last editor	Aku Seppänen
Contributors	UEF (Jyrki Jauhiainen, Mikko Räsänen, Petri Kuusela, Tuomo Savolainen, Aku Seppänen)
Dissemination level	Public (PU)

This Project has received funding from the European Union's Horizon 2020 research and innovation programme under grant agreement no. 764810

History of the changes

Version	Date	Released by	Comments
1.0	30-09-2019	Aku Seppänen	First draft completed
2.0	11-10-2019	Aku Seppänen	Final version
3.0	14-10-2019	Alberto Striolo, Aku Seppänen	Review and minor editorial changes
4.0	15-10-2019	Evghenia Scripnic	Final version and submission

Table of contents

1 Introduction 4
1.1 General context 4
1.2 Deliverable objectives 4
2 Methodological approach 5
3 Summary of activities and research findings 8
3.1 Painted sensing skins in crack detection, planar geometries 8
3.2 Non-planar (3D) sensing skins 10
3.3 Stretchable sensing skin for distributed strain monitoring 12
3.4 Development of computational methods for image reconstruction 15
4 Conclusions and future steps 18
5 Publications resulting from the work described 19
6 Bibliographical references 20

Key word list

Structural health monitoring, damage detection, strain monitoring, electrical resistance tomography, sensing skin, conductive paint, inverse problems

Definitions, acronyms and symbols

Acronyms	**Definitions**
EIT/ERT	Electrical impedance tomography / Electrical resistance tomography
FE	Finite element
FEM	Finite element method
NL–PDPS	Non-linear primal–dual proximal splitting
RGN	Relaxed inexact proximal Gauss-Newton
SHM	Structural health monitoring
TV	Total variation
UEF	University of Eastern Finland

Symbols	**Definitions**
$A(\sigma)$	Regularization functional
$h(\sigma)$	FEM-based forward model of ERT
I	Vector consisting of measured electric current data
I_ℓ	Electric current through the ℓ^{th} electrode
e_ℓ	Surface of ℓ^{th} electrode
L	Number of the electrodes
L_n	Weighting matrix
$\bar{n}$	Outward unit normal
$\bar{r}$	Spatial coordinate vector
σ	Electric conductivity
σ_{ref}	Reference conductivity, or conductivity at the initial state
u	Electric potential
U_ℓ	Electric potential on the ℓ^{th} electrode
w	Step length parameter in RGN algorithm
Ω	Computational domain
z_ℓ	Contact impedance of the ℓ^{th} electrode

1 Introduction

1.1 General context

One of the main goals of S4CE is the assessment of environmental risks in geo-energy sub-surface operations such as carbon capture and sequestration (CCS), production of unconventional hydrocarbons, and enhanced geothermal energy (EGT) production. Among these risks are those caused by fugitive emissions of fluids from subsurface. Because practically all geo-energy operations use structures made of concrete and steel, the possible emission risks are directly linked to durability of these materials and structures, both in operating and abandoned wells.

The S4CE work package 6, *Implementation of Novel Technologies,* is dedicated on developing and testing new instruments for monitoring the wells used in geo-energy operations. This deliverable, D6.2 – *Proof of concept laboratory demonstration of EIT based sensing skin for well cap structures* reports the actions and results of Task 6.2 in WP6 – *Development of sensing skin for geo-energy applications.* In this task, the special focus is on monitoring the integrity of concrete structures in wells used in geo-energy operations.

The novel tool developed in this research is the *sensing skin*, which uses electrically conductive paint applied on the surface of a solid structure to monitor the health of the structure. The electrical conductivity of the paint is imaged using a tomographic technique referred to as *electrical resistance tomography (ERT)*. If successful, the sensing skin will give valuable information on the integrity of the structure – revealing, e.g., surface breaking cracks and other damages on the structure.

While this deliverable describes the laboratory development and testing of the sensing skin technique, its field site implementation will be reported in the upcoming deliverables D7.4 and D7.7 of WP7.

1.2 Deliverable objectives

This deliverable and associated Task 6.2 *Development of sensing skin for geo-energy applications* focus on testing the sensing skin technique in laboratory studies, as well as developing the computational methods required for the image reconstruction in practical applications.

Electrical sensing skin is a versatile tool, which is capable of imaging cracks and other damages on solid surfaces (Hallaji, 2014), presence of Chloride ions (Seppänen, 2017) and temperature distributions (Rashetnia, 2017). In addition, similar techniques have also been shown to be sensitive to change in the pH on the surface (Hou, 2007) and on the strain of the material (Tallman 2017). Many of these monitoring possibilities could potentially be used also in geo-energy applications, such as: rapid detection of cracks in concrete structures of geothermal

wells, or detecting CO2 leakages – high concentration of CO2 on a surface decreases the pH, and thus could potentially be detected with an electric surface sensing system.

To identify the most promising applications of the sensing skin in the geo-energy field, UEF discussed with field site partners and other industrial representatives. Based on these discussions, and on the *S4CE Advisory board's* recommendation in late 2018, an emphasis was put on developing a technique which could provide information on the well bore integrity. A potential method for monitoring the well bore integrity could be one based on imaging strains on surfaces of the metallic casings – the casings undergo thermal expansions during the operations, and if the concrete structures around/between the casings fail, the induced strains can cause permanent damage to the casings. For this reason, in addition to considering crack detection applications, we studied whether painted sensing skins could also be used for monitoring of spatially distributed strains on solid surfaces.

The specific objectives of this deliverable – all addressed in Section 3 – are thus:

- Laboratory testing of the painted sensing skins in laboratory conditions. The purpose of these experiments was to study the effects of different geometries, electrode setups and paint materials on the reconstructions.
- To develop the computational methods used in the image reconstruction so that the sensing skin can be applied to surfaces of arbitrary (non-planar) shapes. Previously, only inaccurate two-dimensional models have been used even for non-planar sensing skins.
- Development of the stretchable sensing skin for distributed strain monitoring.
- Speeding up the image reconstruction in ERT via development of computational methods. This is an important aspect, because before this work, the computation times needed for accurate image reconstruction were too long for online monitoring applications – especially in sensing skins applied to large scale structures.

2 Methodological approach

A sensing skin consists of a thin layer of electrically conductive paint which is applied on the surface of a solid structure. The electrical conductivity of the paint layer is monitored by an electrical imaging technique, electrical resistance tomography (ERT, described briefly below). As ERT is capable of imaging the spatial distribution of the electrical conductivity on the paint layer, it can be used for inferring physical/chemical conditions on the surface. For example, when applied to a surface of a concrete structure; if the concrete cracks, the paint layer ruptures and the local decrease in conductivity will be detected. Recent studies have shown that, in addition to monitoring cracks (Hallaji, 2014), sensing skins can be used for detecting the presence of Chloride ions (Seppänen, 2017) and imaging 2D temperature distributions (Rashetnia, 2017).

Figure 1 illustrates a typical measurement setup in ERT: A set of electrodes is attached on the surface of the object, and using the electrodes, a set of current injections and potential measurements are carried out sequentially. Each set of measurements is then used for reconstructing the conductivity distribution within the target. This image reconstruction problem is mathematically an ill-posed inverse problem – meaning that its classical solutions are non-unique and highly intolerant to measurement noise and modeling errors; hence reconstructing the conductivity requires special computational methods (Kaipio 2006).

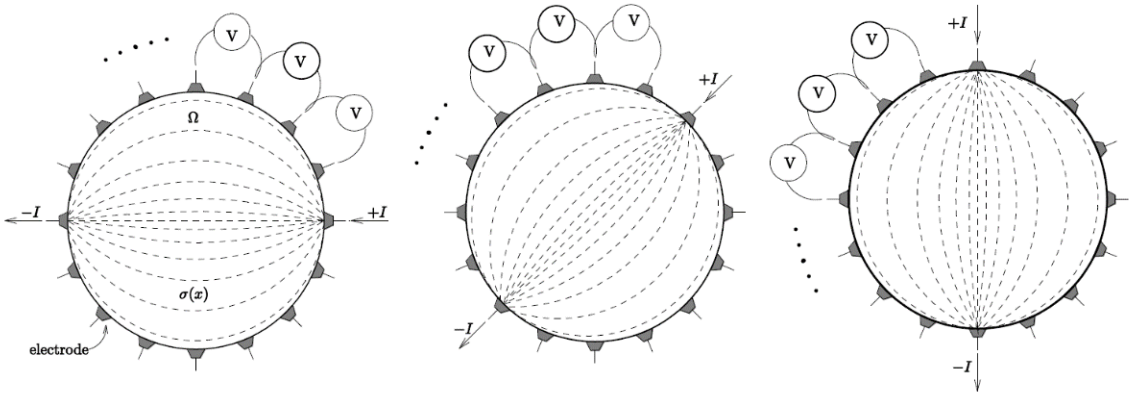

Figure 1: Schematic illustration of a typical measurement setup in ERT. Electric currents (I) are injected through electrodes attached on the perimeter of the object, and voltages (V) between electrodes are measured.

Here, it is worth noticing that our measurement setup has a few properties that differ from a conventional ERT setup:

- While in other applications of ERT electrodes are attached on the surface so that they are in Ohmic contact with the material/structure of interest, in the sensing skin applications, the electrodes are not in contact with the solid structure of interest. Instead, the sensing skin (i.e., the layer of paint) is applied on a surface of an electrically resistive material – such as surface-dry concrete – and the electrodes are only in contact with the sensing skin. If the substrate is conductive – for example, when monitoring the surface of a steel pipe or wet concrete – the surface needs to be insulated by a non-conductive paint before applying the conductive paint layer.
- For this reason, while practically all other applications aim at reconstructing the three-dimensionally distributed conductivity within the object of interest, in the sensing skin application, the thickness of the sensing skin is only in the order of micrometres, and the imaging problem is essentially two-dimensional.
- Although in the schematic pictures in **Figure 1**, electrodes are attached only in the perimeter of the two-dimensional target, the sensing skin application allows also the use of internal electrodes, i.e. electrodes that are attached inside the area of interest. Because the use of internal electrodes improves the resolution of ERT (Rashetnia 2018), they were used in most of the experiments in this project.

- Instead of using current injections and potential measurements, we are using a set of potential excitations and current measurements. This minor difference is due to the properties of the commercial ERT device purchased for the project. In fact, this feature improves the signal-to-noise-ratio of the measurements, since all ERT measurement systems are limited by the maximum potential that can be applied to an electrode.

The most accurate model for the measurements in ERT, referred to as complete electrode model, is of the form (Cheng 1989)

$$\nabla \cdot (\sigma \nabla u) = 0, \quad \bar{r} \in \Omega \tag{1}$$

$$u + z_\ell \sigma \frac{\partial u}{\partial \bar{n}} = U_\ell, \quad \bar{r} \in e_\ell, \ell = 1,2,\dots,L \tag{2}$$

$$\sigma \frac{\partial u}{\partial \bar{n}} = 0, \quad \bar{r} \in \Omega \setminus \bigcup_{\ell=1}^{L} e_\ell \tag{3}$$

$$\int_{e_\ell} \sigma \frac{\partial u}{\partial \bar{n}} dS = I_\ell, \quad \bar{r} \in e_\ell, \ell = 1,2,\dots,L \tag{4}$$

where σ is the electric conductivity, u is the electric potential, $\bar{n}$ is the outward unit normal, U_ℓ , I_ℓ and z_ℓ, respectively, are the potential, current and contact impedance corresponding to electrode e_ℓ, and L is the number of the electrodes.

The image reconstruction is written in the form of a regularized least-squares problem

$$\hat{\sigma} = \arg \min_{0 \le \sigma \le \sigma_{ref}} \{ \| L_n (I - h(\sigma)) \|^2 + A(\sigma) \} \tag{5}$$

where *I* is a vector consisting of the measured electric current data, $h(\sigma)$ is a computational model which maps the electrical conductivity σ to boundary currents. Here, model $h(\sigma)$ is constructed by finite element (FE) approximation of the model (1-4); for details of ERT-FEM, see (Vauhkonen, 1999). Further, L_n is a weighting matrix related to the noise level and $A(\sigma)$ is the so-called regularization functional which can be used for promoting *a priori* known features in the solution. Finally, the constraints of the optimization problem ($0 \le \sigma \le \sigma_{ref}$) are based on the fact that conductivity is a non-negative quantity, and on the assumption that the conductivity of the sensing skin does not increase from the initial conductivity σ_{ref}. This is a valid assumption in cases where sensing skins are used for imaging cracks. In the case of strain imaging, conductivity changes can be positive (local compression) or negative (tension). Note that the initial conductivity σ_{ref} can be estimated on the basis of ERT measurements taken once the sensing skin is installed – i.e., before cracks or strains emerge on the surface.

Figure 2 illustrates the FE meshes used in the modelling (i.e., constructing the forward mapping $h(\sigma)$) corresponding to three geometries. One of the FE meshes corresponds to a planar sensing skin geometry with internal electrodes, and the other two meshes correspond to non-planar geometries.

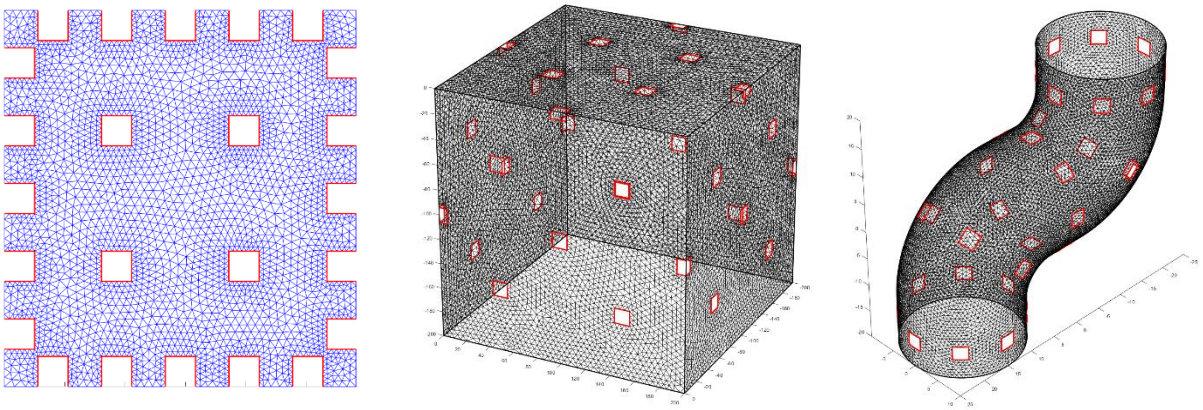

Figure 2: Finite element meshes used in the computational modelling of the ERT measurements with sensing skins. The red lines indicate the locations of electrodes. A 2D geometry with twenty electrodes on the perimeter, and four internal electrodes (left), and 3D geometries: sensing skin applied on five sides of a cube (middle) and on the surface of a pipe (right).

To test the sensing skins experimentally, a 32-channel electrical tomography system was purchased from Rocsole Ldt (www.rocsole.com). This device was used in all the experiments described in Section 3. **Figure 3** shows the measurement system and a measurement setup, where a sensing skin is painted on a solid substrate.

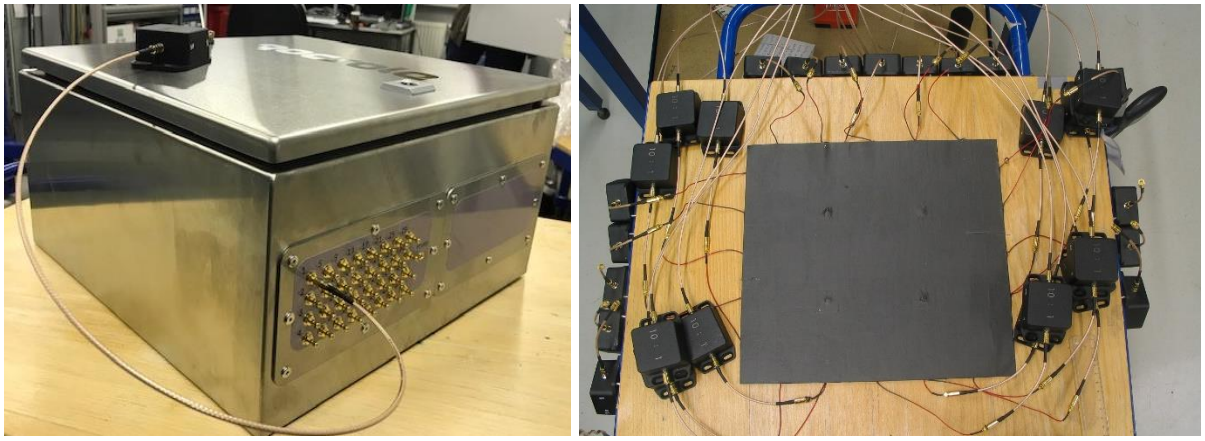

Figure 3: ERT measurement system (manufactured by Rocsole Ltd) used in the experiments (left), and a painted sensing skin applied on a substrate (right).

3 Summary of activities and research findings

This section summarizes the research activities and the results of laboratory testing of the sensing skin. Sections 3.1 and 3.2 consider crack detection applications in different geometries, and Section 3.3 focuses on strain imaging. Finally, Section 3.4 describes the development of computational methods for image reconstruction.

3.1 Painted sensing skins in crack detection, planar geometries

In the first experimental tests, a sensing skin was applied on a plexiglass. The sensing skin was made of commercially available graphite paint that was spray-painted on the plexiglass. Thirty-two electrodes were attached on the sensing skin; four of them were internal

electrodes. The electrodes were connected to the thirty-two channels of the ERT measurement system, and they were all used in the measurements.

The cracks were made on the sensing skin synthetically by scratching the paint with a knife. A total of six stages of cracking were created. **Figure 4** (top two rows) shows the evolution of the crack pattern during the experiment. The thick black lines indicate the locations of the cracks. Note that these lines are drawn on the photographs; the actual cracks were extremely thin, and barely noticeable visually.

Figure 4 (bottom two rows) also shows the ERT-based, reconstructed conductivity distributions corresponding to all six stages of cracking. The reconstructed images are in a very good agreement with the photographs showing the actual crack patterns. Although ERT is not generally a high-resolution imaging modality, in this application, the accuracy is adequate for localizing all the cracks on the surface.

The resolution of the reconstructions is higher than in our previous publications (Hallaji, 2014; Seppänen, 2017); the main reason for this improvement is the use of the new computational methods (non-smooth TV regularization, see Section 3.4). The measurement data from these experiments was used for testing the computational methods that aimed, not only to improving the resolution, but also to speeding up the reconstructions. Moreover, encouraged by the results with the graphite paint in planar geometries, the same measurement system was further used in the experiments in the non-planar geometries.

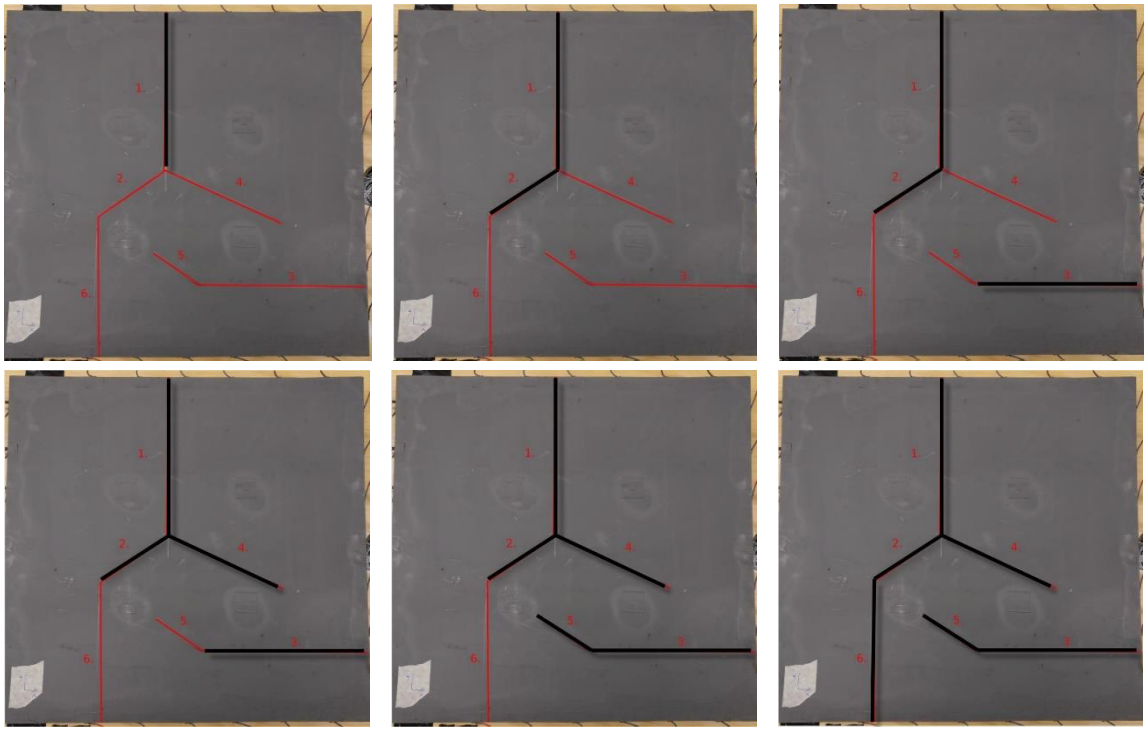

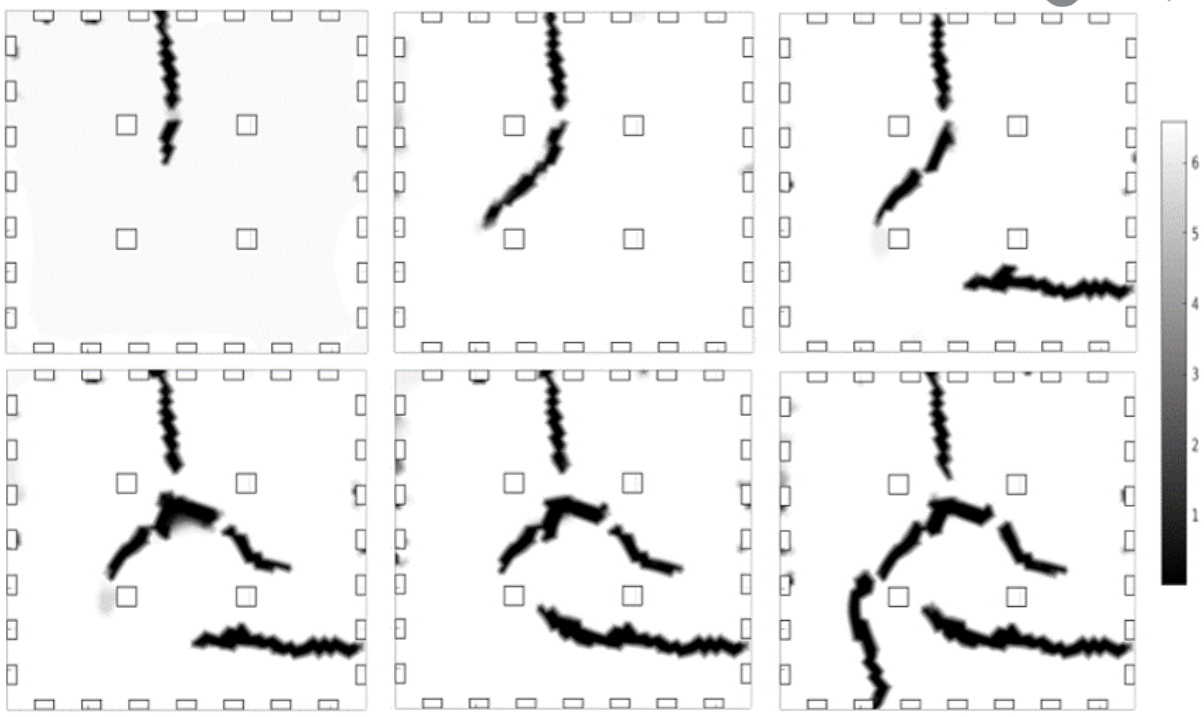

Figure 4: The top two rows show photographs of a sensing skin applied on plexi-glass. Six stages of cracking are marked in the photos with with black lines. The two bottom rows illustrate the ERT-based reconstructions corresponding to six stages of cracking.

3.2 Non-planar (3D) sensing skins

To extend the sensing skin technique to non-planar geometries, which are often present in real applications, the computational model was reformulated. That is, the FE approximation of the model (1—4) was rewritten so that the computational domain Ω follows the surface of an arbitrarily shaped object. **Figure 2** shows two such non-planar geometries.

The non-planar sensing skins were tested both with numerical simulations and experimentally. **Figure 5** shows the results of one simulation study. Here the surface of a curved pipe was assumed to be covered by conductive paint, and a synthetic crack was simulated on it (**Figure 5**, left). The reconstructed image of the conductivity (**Figure 5**, right) indicates the location of the crack with very good accuracy.

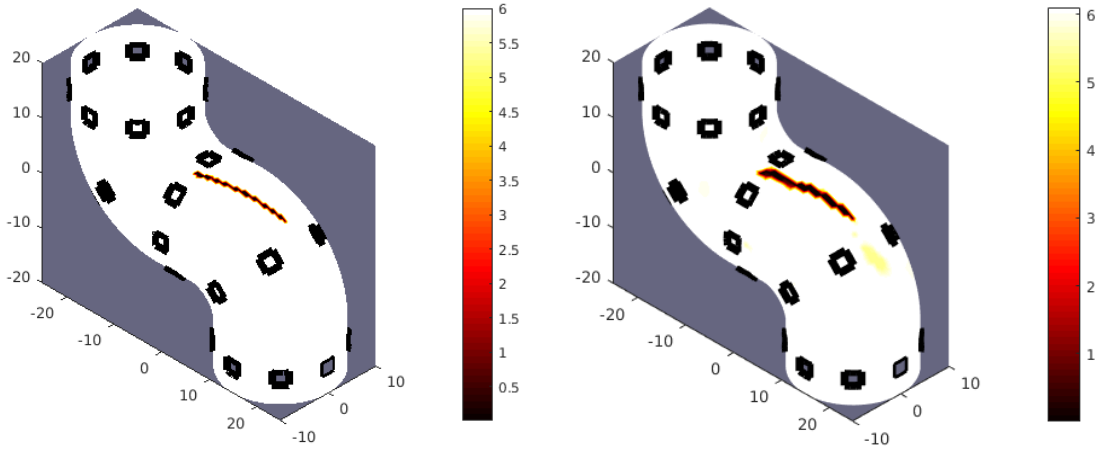

Figure 5: Numerical test of the non-planar (3D) sensing skin. Left: True conductivity distribution of a sensing skin on the cracked surface of a curved pipe. Right: EIT-based reconstruction of the conductivity.

For the experimental study, a graphite-based sensing skin was painted on the outer surface of a plastic box (**Figure 6**, left column). Five sides of the box were painted, and thirty-two electrodes were placed on it. Again, cracks were made on the sensing skin synthetically by scratching the paint. Four stages of cracking were considered. The segments of cracks scratched between different stages are highlighted with different colours in the photographs of **Figure 6** (first crack is drawn with red colour, the second with blue; the third and fourth crack are marked with yellow and green colour, respectively). Note that the last two cracks were on different side of the cube than the first two cracks.

Figure 6 (two rightmost columns) also shows the reconstructions of the electrical conductivity corresponding to all four stages of cracking. Again, all cracks are detected rather accurately. Note here that the reconstruction of the last stage of cracking (**Figure 6**, bottom right) does not show the entire extent of the fourth crack only because of the view angle (part of the crack is behind the cube). An animated visualization of the 3D geometry would reveal the true shapes of all cracks on the surface.

Numerical simulations and the experimental study suggest that the developed computational tools for the 3D geometries are feasible and allow for monitoring of non-planar surfaces.

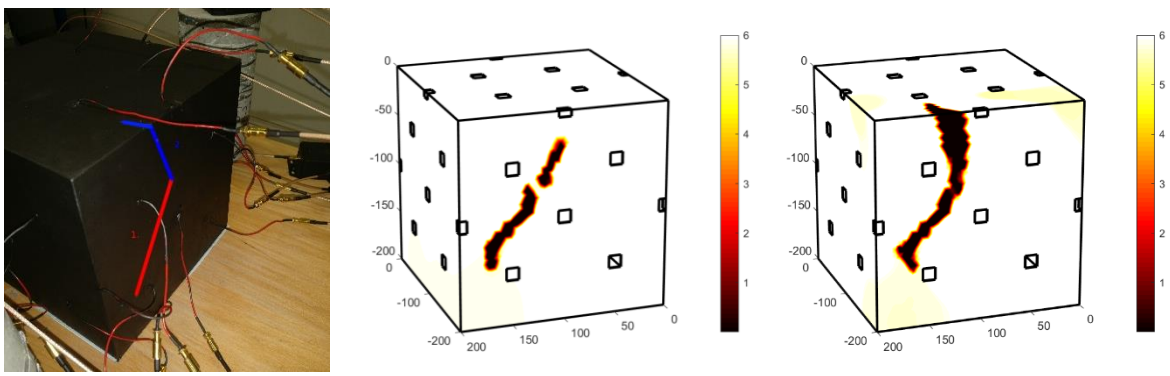

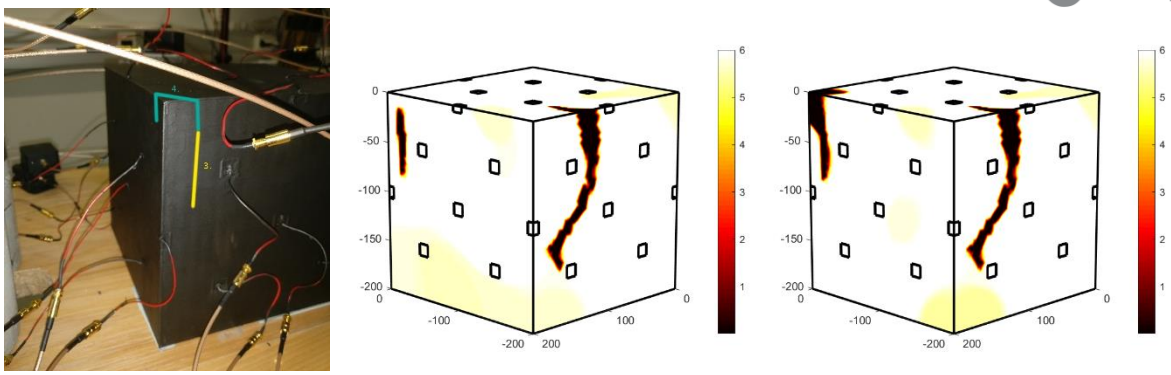

Figure 6: Experimental test of the non-planar (3D) sensing skin. Left column: Photos of a box with five of its surfaces covered with sensing skin. In the first photo, the red and blue line indicate the locations of the first two cracks scratched on the sensing skin. The yellow and green line in the second photo represent the third and fourth crack, respectively. The second and third column illustrate the reconstructions of the sensing skin conductivity at these four stages of cracking.

3.3 Stretchable sensing skin for distributed strain monitoring

This part of the research was started by testing a variety of materials that could potentially be used for strain monitoring. A suitable sensing skin material for this purpose should fulfil the following requirements:

- It should be electrically conductive, and its conductivity should be in a range suitable for the ERT measurement system (to ensure feasible quality with the device currently used, the resistances between electrode pairs should be in the order of kilo-ohms).
- It should be flexible, and easy to fix to a substrate surface.
- It should respond to stretching by decrease of electric conductivity.

Many of the tested paint materials turned out to be either non-conductive or too conductive. One of the materials (a conductive rubber sheet) had otherwise suitable electrical properties, except that its conductivity turned out be *anisotropic* – a feature, which might even be beneficial in some cases, but because it also makes the interpretation of the data more challenging, the material was discarded.

Finally, a suitable material for the stretchable sensing skin was made in-house, by mixing graphite powder to a rubber paint (**Figure 7**, left). The conductivity of this mixture can be controlled by choosing the portion of the conductive component, graphite powder, in the mixture. Similarly to the graphite paint, this paint mixture is easy to spread either by using a brush or by spraying. Most importantly, the series of tests carried out with stripes of the flexible paint showed that the conductivity of the paint – indeed – changes when it's stretched.

Figure 7: Left: Ingredients of a stretchable sensing skin: graphite powder and rubber paint. Right: Stretchable sensing skin applied on a (non-conductive) rubber sheet. Twenty electrodes are attached near the boundaries of the sensing skin.

To test the ability of ERT to detect deformations of the flexible sensing skin, a layer of the paint mixture was applied on a non-conductive rubber sheet. The first tests, where entire sensing skin was stretched by grabbing it from opposite ends, did not yield reconstructions of a very good quality; instead, multiple artefacts were observed in the reconstructions, yet they also showed somewhat strong conductivity changes due to stretching. The two major causes of the artefacts turned out be: 1) the additional deformation of the sensing skin caused by the compression caused by grabbing the sheet, and 2) unstable contact impedances of the electrodes caused by stretching of the conductive paint around them.

The former problem was avoided in the sequel, by avoiding the compression the sensing skin in the stretching tests. The latter issue, unstable contact, required additional, application-specific development in the computational methods: The image reconstruction was written in the form of a non-linear difference imaging problem as in (Smyl, 2018), with a modification that takes into account that the contact impedances of the sensing skin may change from the reference state when the sensing skin is stretched.

To test the sensitivity of the stretchable sensing skin to moderate deformations that are local, the technique was tested with a setup shown in **Figure 8**. The photographs in the left column correspond to two situations where the sensing skin was deformed by placing weights on it. First, one plastic weight (500 g) was placed in the top right corner; at the second stage, another, identical weight was added in the bottom left corner. The reconstructed images (**Figure 8**, right column) show, at least approximately the locations of the weights. In both locations, the reconstructed images indicate a decrease in conductivity.

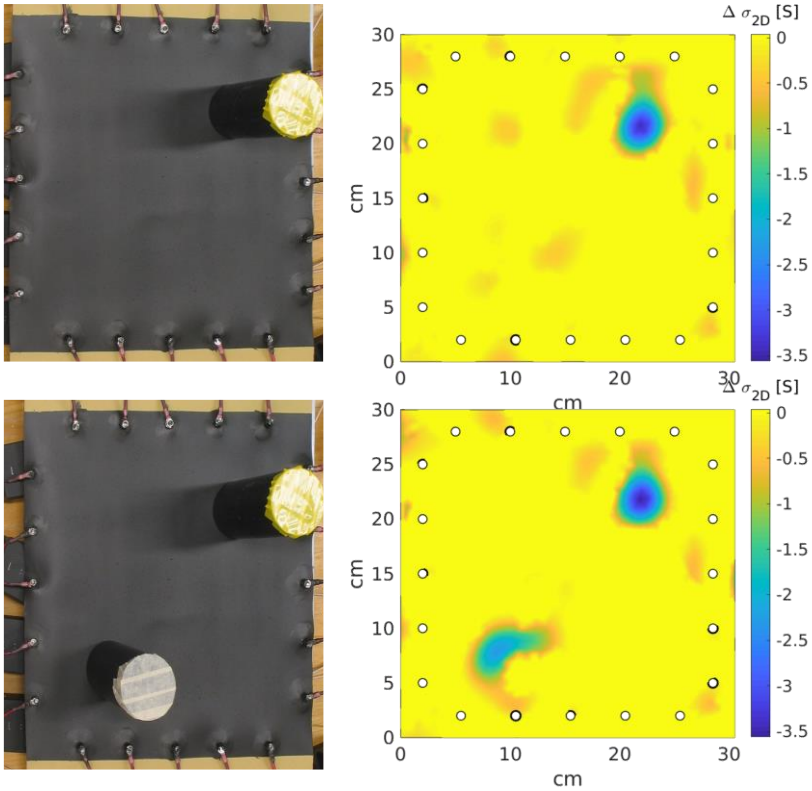

Figure 8: Results of experiments with a stretchable sensing skin 1/2. Left column: Photos of two measurement setups. Right column: Reconstructed conductivities of the sensing skin while the weights were on it.

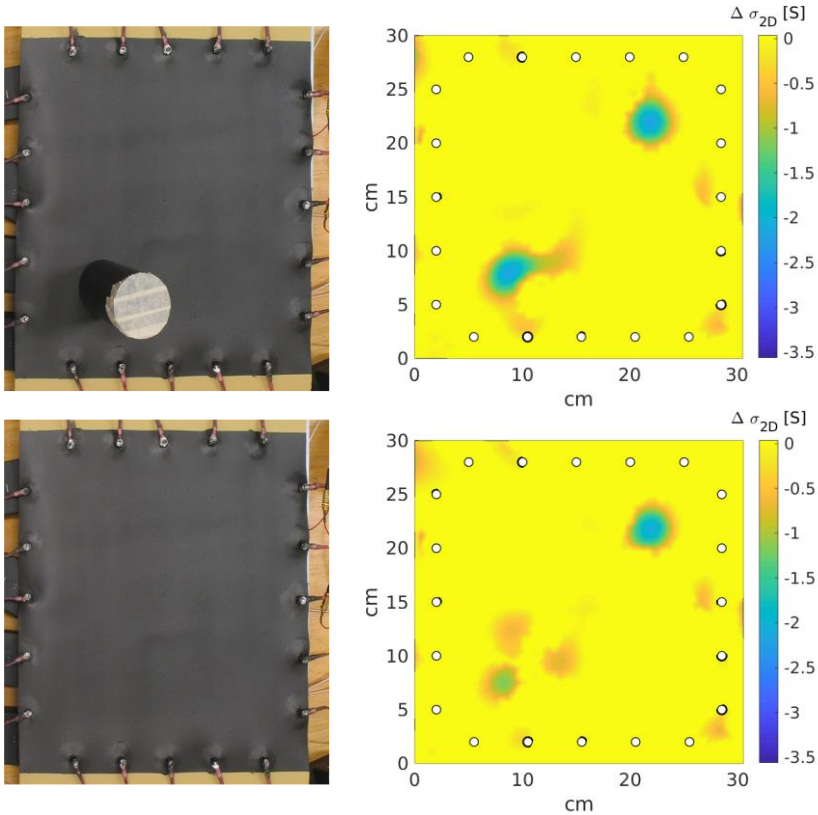

Figure 9: Results of experiments with a stretchable sensing skin 2/2. Left column: Photos of two measurement setups. Right column: Reconstructed conductivities of the sensing skin.

Next, the two weights were removed from the table one by one. First, the weight in the top right corner was removed, and then, the one in the bottom left. The reconstructed images are depicted in **Figure 9**. Interestingly, the locations where the weights had been before their removal still show lower conductivity in the reconstructions, yet these conductivity inhomogeneities are not as strong as the inhomogeneities while the weights were still on. This is a result of a memory/relaxation effect in the sensing skin conductivity: The deformation of the stretchable material does not recover immediately; for this reason, also the local conductivity change caused by the weight recovers slowly.

Overall, the results of **Figure 8** and **Figure 9** demonstrate that the stretchable sensing skin enables detecting local deformations on surfaces. In the next experiments, the sensing skins will be stretched locally in a controlled manner; the final aim being at quantifying the strain field on the surface. This, of course, requires experimental calibration of the sensing system and/or modelling the dependence between electrical conductivity and deformations.

3.4 Development of computational methods for image reconstruction

As noted in Section 2, the image reconstruction problem of ERT is an ill-posed inverse problem. The regularization functional $A(\sigma)$ in Equation (5) has a crucial effect on the reconstructed images. In crack detection applications, a suitable choice for $A(\sigma)$ is a total variation (TV) model, which promotes sharp edges in the spatial distribution of the conductivity σ (Kaipio, 2006). This choice, on the other hand, makes the image reconstruction problem cumbersome, because the TV model is a non-smooth function.

To overcome the problem of non-smoothness, the regularization functional $A(\sigma)$ is often replaced by its smoothed approximation (Hallaji 2014), which allows for the use of conventional optimization methods, such as Newton iteration. This approximation, however, lowers the contrast of the reconstructed images (Jauhiainen 2019). To avoid smoothing, state-of-the-art non-convex, non-smooth optimization methods were adopted and further developed for the problem at hand.

The developed non-convex, non-smooth optimization method is referred to as *relaxed inexact proximal Gauss-Newton* (RGN). In our manuscript (Jauhiainen 2019), RGN is tested with various numerical simulations and experimental studies. The new method was found to be advantageous over existing optimization methods in the TV-regularized ERT problems. **Figure 10** shows a comparison of the convergence of the developed RGN with different step length parameters w and the current state-of-the-art method referred to as *non-linear primal–dual proximal splitting* (NL-PDPS) optimization (Valkonen, 2014; Clason, 2019). The plot in **Figure 10** (left) shows that when using step length parameters w that lead to convergence (i.e., $w \neq 1$), RGN converges in about 10-20 iterations while in NL-PDPS the required iteration number is in the order of 10^3-10^4. Consequently, the computation times (plotted in **Figure 10**, right) required by NL-PDPS are about three orders of magnitude longer

than with RGN. This is a result of practical significance for on-line monitoring applications: The computation time of RGN is about 200-300 seconds, while NL-PDPS requires 10^5s ≈ 28 hours!

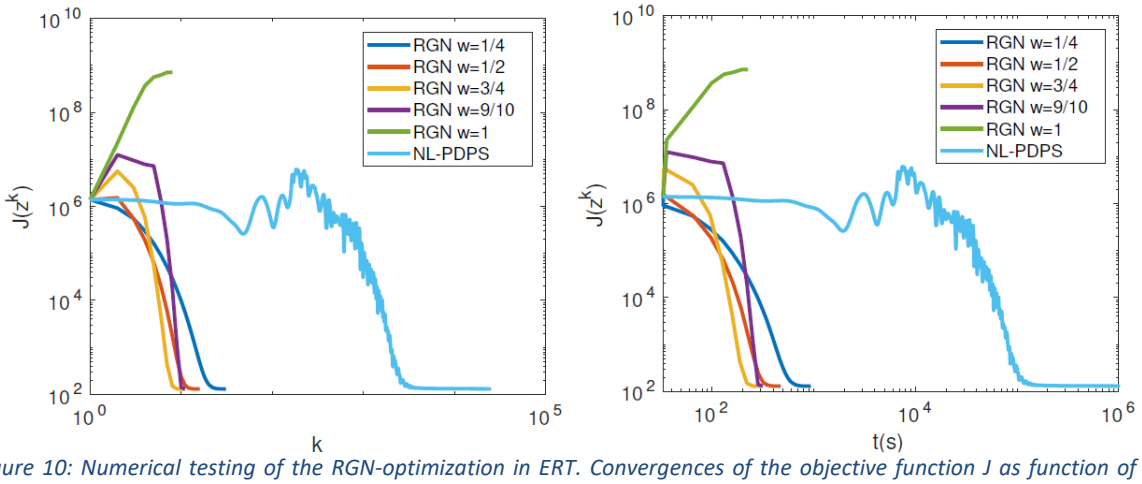

Figure 10: Numerical testing of the RGN-optimization in ERT. Convergences of the objective function J as function of the iteration number k (left), and computation time t (right) for the RGN-algorithm corresponding to five relaxation parameters w and for NL–PDPS.

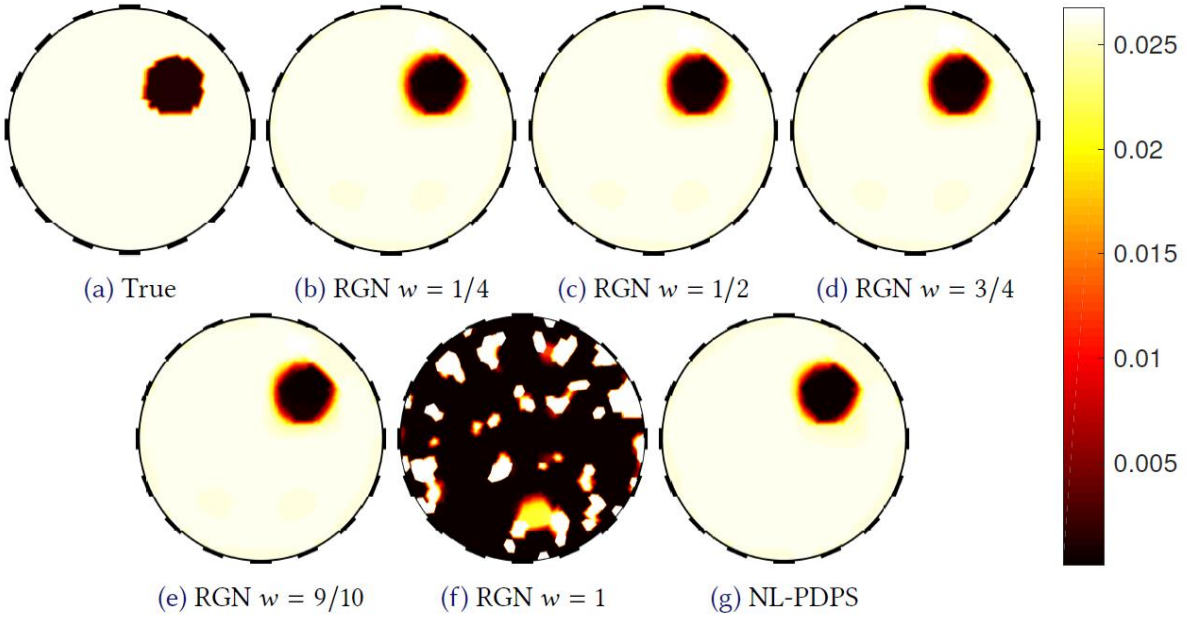

Figure 11: Numerical testing of the RGN-optimization in ERT. True conductivity (a), RGN–based reconstructions corresponding to five relaxation parameters w (b)–(f), and the NL–PDPS–based reconstruction (g).

Figure 11 shows the reconstructed images obtained using RGN with different step lengths and the NL-PDPS -based reconstruction. All reconstructions except the one corresponding to non-converged case (w=1) are close to the true conductivity distribution which is also shown in the figure. The differences between the RGN- and NL-PDPS based reconstructions are very small. In conclusion, in this simulated test case, RGN results in practically the same reconstruction accuracy as NL-PDPS in a computation time that is orders of magnitude shorter than that of NL-PDPS.

In addition to simulation studies, the developed optimization method was also tested in multiple experimental cases. **Figure 12**-**Figure 13** represent an experiment with a sensing skin

(same as the second stage of cracking in the **Figure 4**). Here, RGN was applied to the smoothed version of the TV-regularized ERT-reconstruction. The main purpose of this test was to study how the RGN compares with a conventional Newton iteration. Note that this comparison can only be carried out with the smoothed TV-functional, because the conventional Newton's method is not applicable to non-smooth optimization.

The RGN -based ERT reconstructions converge faster than the conventional Newton iteration, yet the difference is not as large as in the RGN vs. NL-PDPS comparison of the previous example. The reconstructed images are shown in **Figure 13**. The quality of all reconstructions is on the same level. It is also worth noticing that in these images, the contrast is slightly lower than the corresponding reconstruction in **Figure 4**; this is a result of using smoothed version of TV – the reconstructions in **Figure 4** were computed with RGN without smoothing the TV.

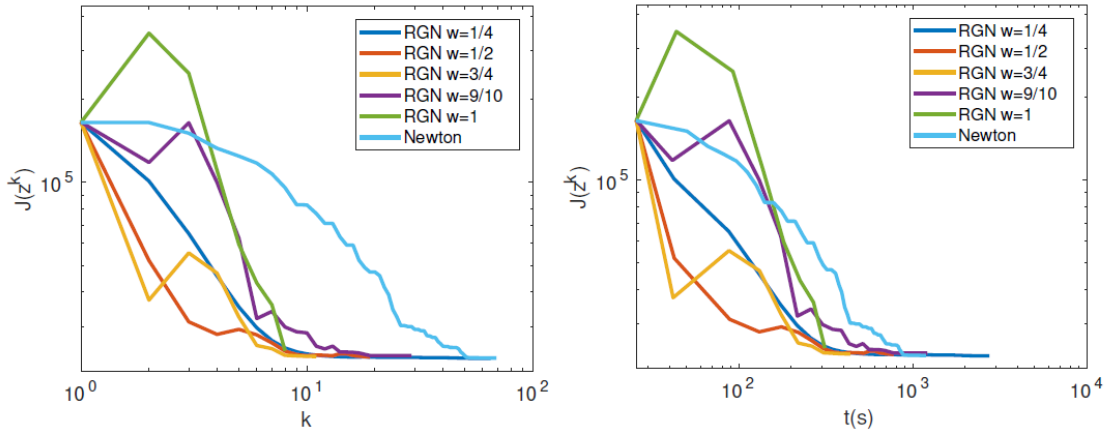

Figure 12: Experimental testing of the RGN-optimization in ERT: sensing skin case. Convergences of the objective function J as function of the iteration number k (left), and computation time t (right) for the RGN-algorithm corresponding to five relaxation parameters w and for NL–PDPS.

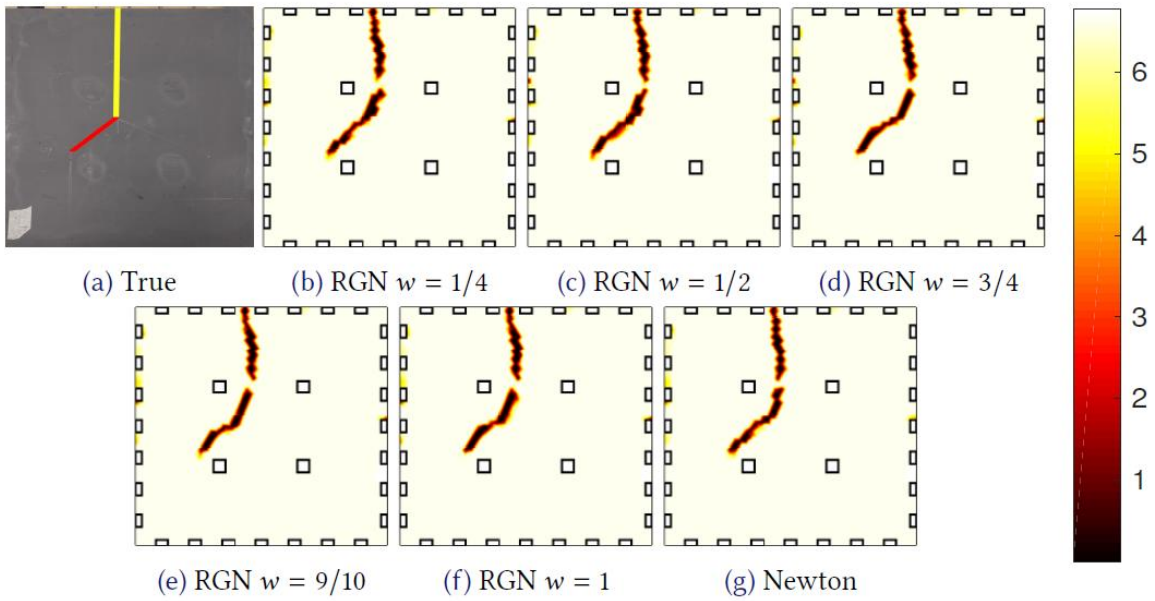

Figure 13: Experimental testing of the RGN-optimization in ERT: sensing skin case. Photo of the sensing skin (crack highlighted) (a), RGN–based reconstructions corresponding to five relaxation parameters w (b)–(f), and the Newton–based reconstruction (g).

4 Conclusions and future steps

In order to assure the safety of geo-energy operations, new instruments for monitoring the well structures are needed. Notably, the potential degradation of sealing structures made of concrete is of great importance. New tools are needed for monitoring the condition of casings in operating wells. This deliverable reported the results of laboratory tests that aim at introducing a new imaging tool for these purposes: electrical resistance tomography (ERT) -based sensing skin. To complement laboratory testing, a significant effort was put on the development of computational methods in the ERT image reconstruction; the particular aim of this work was speeding up the computations so that sensing skin would become applicable to online monitoring.

The results of this deliverable demonstrate that ERT allows detection of complex crack patterns, especially when internal electrodes are used. The numerical and experimental studies show that the sensing skin technique is applicable to non-planar surfaces. Moreover, the studies with painted, flexible sensing skin suggest that the technique can also be used for imaging deformations, or strains, on the solid surfaces. Finally, the computational methods (especially the RGN optimization) enable a significant speed-up of the image reconstruction.

The next steps of this research are:

- Field site testing of the sensing skin. The first tests are scheduled for October-November 2019 in St Gallen field site. The emphasis of the tests will be in the concrete integrity applications. Both the cellar walls and the concrete structure around the top part of the casing will be considered. These tests will be carried out in S4CE work package 7, and the results will be reported in the upcoming deliverables D7.4 and D7.7.
- Simultaneously, in WP7, research is done in testing a new measurement technique, which could potentially enable continuous monitoring with low costs. If successful in laboratory tests, the technique will also be tested in the field site.
- The development of the flexible sensing skin for the strain measurement will also be continued. Here, the next steps will be 1) carrying out a controlled test, where the sensing skin is stretched gradually, and the deformations are recorded. This will the first step towards *quantitative* strain measurement with sensing skin. 2) The second step in this work will be connecting ERT imaging with the strain quantitatively, by modeling the dependence of the electrical conductivity and the strain.

5 Publications resulting from the work described

Journal papers (in preparation):

J. Jauhiainen, P. Kuusela, A. Seppänen, T. Valkonen: "Relaxed inexact proximal Gauss — Newton for high dimensional non-convex non-smooth problems – applications to electrical impedance tomography", *In Preparation*, will be submitted to *SIAM Imaging Science* in 2019.

Two other manuscripts will be submitted for review in scientific journals in 2020:

- The first paper focuses on strain imaging using stretchable sensing skin.
- The second paper demonstrates the application of the non-planar sensing skin.

Conference presentations/invited talks/abstracts:

A. Seppänen: "Electrical Impedance Tomography, non-destructive testing and Bayesian inverse problems", Invited talk in *Technical University of Denmark*, March 13, 2018.

A. Seppänen, G. Gonzalez, V. Kolehmainen, M. Pour-Ghaz: "Total variation priors in electrical impedance tomography", *SIAM conference in Imaging Science*, Bologna, Italy, June 5-8, 2018.

A. Seppänen, A. Voss, J. Jauhiainen, P. Kuusela, T. Savolainen, M. Pour-Ghaz: "Electrical tomography for material characterization and structural health monitoring", *The International Carbon Conference, Reykjavík*, Iceland, September 10-14, 2018.

S. Sampethai, A. Angulo, F. Wandji, A. Seppänen, J. Jauhiainen, M. Pour-Ghaz, M Puddu, G. Mikutis, R. Pini, P. Capuano, M. Falang: "Science for Clean Energy: Implementation of Novel Technologies", *The International Carbon Conference*, Reykjavík, Iceland, September 10-14 2018.

A. Seppänen: "Non-linear difference imaging", *9th International Congress on Industrial and Applied Mathematics*, Valencia, Spain, July 15-19, 2019.

A. Seppänen: "EIT based sensing skin for large-scale structural health monitoring", *Applied Inverse Problems Conference*, Grenoble, France, July 8-12, 2019.

J. Jauhiainen, P. Kuusela, A. Seppänen, T. Valkonen: "An inexact relaxed Gauss–Newton applied to electrical impedance tomography", *International conference on continuous optimization*, Berlin, Germany, August 5-8, 2019.

6 Bibliographical references

K-S. Cheng, D. Isaacson, J. C. Newell, and D.G. Gisser. "Electrode models for electric current computed tomography." IEEE Transactions on Biomedical Engineering, 36: 918-924, 1989.

Clason, Mazurenko & Valkonen, Acceleration and global convergence of a first-order primal-dual method for nonconvex problems, SIAM Journal on Optimization 29: 933–963, 2019.

M. Hallaji, A. Seppänen, M. Pour-Ghaz: “Electrical impedance tomography-based sensing skin for quantitative imaging of damage in concrete”, Smart Materials and Structures, 23: 085001, 2014.

T-C Hou, K.J. Loh and J.P. Lynch: “Spatial conductivity mapping of carbon nanotube composite thin films by electrical impedance tomography for sensing applications”, Nanotech, 18(31): 315501, 2007.

J. Jauhiainen, P. Kuusela, A. Seppänen, T. Valkonen: "Inexact relaxed gauss–newton for high dimensional non-convex non-smooth problems – application to electrical impedance tomography”, *In Preparation*, will be submitted to *SIAM Imaging Science* in 2019.

J. Kaipio, E. Somersalo. ”Statistical and computational inverse problems” Vol. 160. Springer Science & Business Media, 2006.

R. Rashetnia, D. Smyl, M. Hallaji, A. Seppänen, M. Pour-Ghaz: “Detection and localization of changes in two-dimensional temperature distributions by Electrical Resistance Tomography”, Smart Materials and Structures, 26: 115021, 2017.

R. Rashetnia, O. Khalaf Alla, G. Gonzalez-Berrios, A. Seppänen, M. Pour-Ghaz: “Electrical Resistance Tomography Based Sensing Skin with Internal Electrodes for Crack Detection in Large Structures”, Materials Evaluation, 76: 1405-1413, 2018.

A. Seppänen, M. Hallaji, M. Pour-Ghaz: “A functionally layered sensing skin for detection of corrosive elements and cracking”, Structural Health Monitoring, 16: 215–224, 2017.

D. Smyl, M. Pour-Ghaz, A. Seppänen: “Detection and reconstruction of complex structural cracking patterns with electrical imaging”, NDT & E International, 99: 123-133, 2018.

T.N. Tallman, S. Gungor, K.W. Wang, C.E. Bakis: “On the inverse determination of displacements, strains, and stresses in a carbon nanofiber/polyurethane nanocomposite from conductivity data obtained via electrical impedance tomography”, *Journal of Intelligent Material Systems and Structures* 28: 2617-2629, 2017.

T. Valkonen: "A primal–dual hybrid gradient method for nonlinear operators with applications to MRI." Inverse Problems 30: 055012, 2014.

P.J. Vauhkonen, M. Vauhkonen, T. Savolainen, J.P. Kaipio: “Three-dimensional electrical impedance tomography based on the complete electrode model IEEE Trans. Biomed. Eng. 46: 1150–60, 1999.